frontiers | Frontiers in Mechanical Engineering

TYPE Original Research
PUBLISHED 07 January 2026
DOI 10.3389/fmech.2025.1716347

OPEN ACCESS

EDITED BY
Kapil Panchal,
Elliott Company, United States

REVIEWED BY
Thiyam Tamphasana Devi,
National Institute of Technology, Manipur, India
Jinbo Chen,
East Carolina University, United States
Xianshi Fang,
Shenyang Polytechnic College, China
Catur Harsito,
Sebelas Maret University, Indonesia

*CORRESPONDENCE
Pingyang Dong,
dongpingyang7@163.com
Guangtai Shi,
18011107346@163.com

RECEIVED 02 October 2025
REVISED 03 December 2025
ACCEPTED 04 December 2025
PUBLISHED 07 January 2026

CITATION
Dong P, Shi G, Xiao Y, Wen H, Lv W and Peng X (2026) Multi-objective optimization of a multiphase pump booster unit for enhanced hydraulic performance.
Front. Mech. Eng. 11:1716347.
doi: 10.3389/fmech.2025.1716347

Multi-objective optimization of a multiphase pump booster unit for enhanced hydraulic performance

Pingyang Dong[1]*, Guangtai Shi[1]*, Yexiang Xiao[2], Haigang Wen[1], Wenjuan Lv[1] and Xiaodong Peng[1]

[1]Key Laboratory of Fluid and Power Machinery, Xihua University, Ministry of Education, Chengdu, China, [2]State Key Laboratory of Hydroscience and Department of Energy and Power Engineering, Tsinghua University, Beijing, China

As key equipment in oil and gas transmission systems, multiphase pumps are crucial for ensuring a closed oilfield collection and transmission. The booster unit as the core component of the multiphase pump, has blade shapes that significantly impact the pump efficiency and its gas-liquid mixing performance. To enhance the efficiency of the booster unit and improve its gas-liquid mixing, this study first employed an optimal Latin hypercube design to sample blade shape parameters and establish a design library. The effects of these parameters were systematically investigated via numerical simulation. Subsequently, an approximate prediction model was developed and integrated into a multi-objective optimization framework to identify Pareto-optimal blade configurations. Following optimization, the pump efficiency increased from 52.60% to 54.56% (a 3.59% improvement), while the gas uniformity at the impeller outlet decreased from 0.3229 to 0.3040 (a 6.22% reduction). Comparative analysis of internal and external characteristics confirmed improved gas dispersion and more refined flow field structures within the optimized booster unit. The proposed methodology integrates advanced sampling, modeling, and optimization techniques, providing a systematic and efficient strategy for the performance-driven design of multiphase pump blades. This framework offers significant potential for enhancing the hydraulic performance and operational stability of such critical transport equipment.

KEYWORDS

blade multiphase pump, booster unit, hydraulic performance optimization, iSIGHT platform, multi-objective optimization

1 Introduction

As a key component in oil and gas transmission systems, the blade multiphase pump has become a research hotspot owing to its compact structure, wear resistance, and adaptability to various working conditions (Longxin and Zhifeng, 2019; Lirong et al., 2022; Zhou et al., 2024). However, under multiphase flow conditions, flow separation and gas content variations caused by the interphase slip effect, triggered by the high-speed rotation of the impeller, seriously affect the pump's operational stability. To address this issue, researchers have studied the structural and operational parameters of pumps. Tang et al. (2023) demonstrated that a blade tip groove structure can effectively improve the hydraulic efficiency of multiphase pumps. Wen et al. (2022) discovered that as the tip gap increased, the leakage vortices at the tip gradually became more pronounced through their investigation of different leaf tip

gaps. Suh et al. (2017) found that the flow characteristics of the rear stage differ from those of the front stage, suggesting that pump performance can be enhanced through second-stage design optimization. Han et al. (2024a) observed significant performance improvements when the blade-inclination angle exceeded 2°. Wang et al. (2024) revealed that the effect of the blade outlet angle varies under pure water and high gas content conditions, indicating that structural parameters must dynamically match the flow regime. In terms of operating parameters, You and Peng. (2023) addressed varying the gas content by adjusting the pump's operating speed.

Although the above research has improved the performance of blade multiphase pumps under specific conditions through structural and operational optimization, the design theory remains largely based on the framework and experience of single-phase pumps. This results in deviations under multiphase operating conditions, making it difficult to meet the actual project requirements. To overcome these challenges, researchers have focused on optimizing the core components of multiphase pumps. In impeller optimization, Zhang et al. (2017) applied a quasi-three-dimensional hydraulic design, boundary vortex diagnosis, and a genetic algorithm to improve impeller pressure distribution and suppress gas-liquid separation. They further optimized the load parameters and high-pressure edge angle using the response surface method and genetic algorithm, showing that the blade winding angle and control parameters significantly affect the pump efficiency and gas uniformity (Zhang et al., 2022a; Zhang et al., 2022b). Han et al. (2024b) reduced the radial and counter pressure gradients in the impeller channel by adjusting the flap deflection angle and length. Wang et al. (2024) enhanced the pressure-boosting capacity and efficiency of a screw axial multiphase pump under pure water conditions by modifying the outlet angle of the impeller blades. Liu et al. (2020) predicted the velocity bending moment of guide vanes downstream in the flow field based on the Oseen vortex theory and optimized the entry angle of the next impeller blades.

In terms of guide blade optimization, Ge et al. (2023) used impeller blade load as the optimization variable to improve guide blade performance and overall pump efficiency. Li et al. (2020) found that decreasing the guide blade diameter along the radial direction significantly increased the head and efficiency. Additionally, Shi et al. (2021) improved the head and efficiency through orthogonal tests on five pump parameters and filtered the results using a weighting function. Liu et al. (2020), Liu et al. (2018) also performed orthogonal optimization of the impeller and guide blade design parameters to enhance multiphase pump delivery performance. Building on this, Peng et al. (2022a) Peng et al. (2022b) designed experiments and constructed an approximate model using a sparse grid method, followed by multi-objective genetic algorithm optimization, significantly improving the efficiency under large mass flow conditions.

When optimizing impeller and guide blade designs, optimization platforms have become popular owing to their efficiency and ease of use. Chen et al. (2024) used an adaptive sparse grid and multi-objective genetic algorithm to optimize pressurization and efficiency under pure water conditions. Gu et al. (2025) employed a backpropagation neural network combined with a non-dominance sorting genetic algorithm to enhance the aerodynamic performance of centrifugal pumps.

In summary, prior research on multiphase pumps has largely focused on the individual optimization of either impellers or guide blades, with limited studies addressing the joint optimization of the entire booster unit. Furthermore, although the NCGA is widely applied in the pharmaceutical field, its use in optimizing multiphase pump systems is rare. Therefore, to address these research gaps, this study used a self-developed booster unit of a multiphase pump as the research object. By integrating the Workbench and Isight optimization platforms, multi-three-dimensional inverse design, experimental design methods, numerical simulation, response surface method, and genetic algorithms can be achieved. The Pareto front solutions generated by the Nonlinear Constrained Genetic Algorithm (NCGA), MOPSO, and NSGA-II algorithms are compared to identify the most suitable multi-objective approach for pump optimization. The variations in the internal and external performance characteristics of the multiphase pump before and after optimization were thoroughly analyzed. The study results provide a theoretical foundation and novel methodological framework for the integrated optimal design of multiphase pump booster units.

2 Geometric and design parameters

2.1 Physical model

A self-developed single-stage blade multiphase pump booster unit was considered as the object of study. The geometric parameters of the booster unit are listed in Table 1, the design parameters are listed in Table 2, and the numerical model of the blade multiphase pump is illustrated in Figure 1.

2.2 Mesh Segmentation and irrelevance verification

The inverse design of the impeller and guide blades was completed using the CFturbo design software. Structured meshes for the impeller and guide blades were generated using ANSYS TurboGrid. The inlet and outlet sections of the computational model were designed using NX 3D modeling software and meshed with hexahedral structured grids using ANSYS ICEM. The computational domain mesh is shown in Figure 2.

An appropriate number of mesh elements is essential to ensure the time efficiency and accuracy of numerical simulations. Therefore, grid-independence validation was conducted using five mesh configurations under pure water conditions at a rated flow rate of 200 m^3/h, as shown in Table 3. From Table 3, it can be seen that as the mesh density increased, the variation in both the relative head and relative efficiency remained within 1.5%. Because the fourth and fifth mesh configurations showed no significant improvement in solution results, and considering the trade-off between computation time and accuracy, the third mesh configuration—with 3.23 million elements, was selected for the simulation.

TABLE 1 The geometric parameters of booster unit of blade multiphase pump.

Geometric parameter	Notation	Unit	Numerical value
Number of impeller blades	Z_1	(–)	3
Number of guide blades	Z_2	(–)	11
Outside diameter	D	mm	256
Impeller inlet angle	α_h/α_s	°	7.8/4.5
Impeller outlet angle	β_h/β_s	°	28/20
Guide blade inlet angle	α_h/α_s	°	0
Guide blade outlet angle	β_h/β_s	°	28

TABLE 2 Design parameters of booster unit of blade multiphase pump.

Design parameters	Notation	Unit	Numerical value
Design flow rate	Q	m^3/h	200
Design speed	N	rpm	3,000

2.3 Numerical methods

To ensure consistent performance benchmarking of the single-stage multiphase pump pressure unit before and after optimization, the baseline shear stress transport (*SST*) turbulence model was retained. This formulation integrates the $k-\omega$ boundary layer resolution with $k-\omega$ free-stream robustness while explicitly resolving the shear stress effects in multiphase transport. For multiphase modeling, the Euler-Euler approach was adopted, using identical gas-liquid conditions as the operational prototype. This framework solves the coupled momentum and continuity equations per phase using interphase exchange coefficients, representing an established methodology for pump CFD simulations.

The core governing equation of the Shear Stress Transport (SST) model is given by Equations 1, 2.

$$\frac{\partial}{\partial t}(\rho k)+\frac{\partial}{\partial x_j}(\rho k v_j)=\frac{\partial}{\partial x_j}\left[\left(\nu+\frac{\nu_t}{\sigma_k}\right)\frac{\partial k}{\partial x_j}\right]+G_k-\beta\rho k\omega \quad (1)$$

$$\frac{\partial}{\partial t}(\rho\omega)+\frac{\partial}{\partial x_j}(\rho v_j\omega)=\frac{\partial}{\partial x_j}\left[\left(\mu+\frac{\mu_t}{\sigma_\omega}\right)\frac{\partial\omega}{\partial x_j}\right]+G_\omega-\beta\rho\omega^2+D_\omega \quad (2)$$

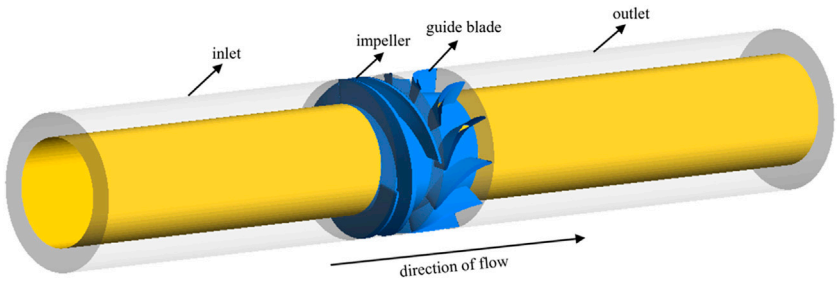

FIGURE 1
Numerical model of blade multiphase pump.

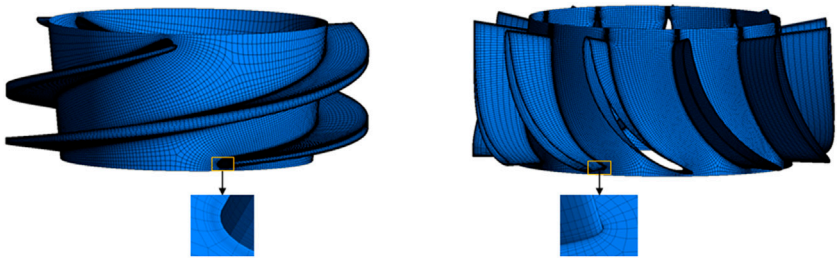

FIGURE 2
The grid of computational domain.

TABLE 3 Mesh independence verification.

Parameter	Grid 1	Grid 2	Grid 3	Grid 4	Grid 5
Grid numbers	2,446,130	2,864,122	3,232,239	3,503,130	421,001
Head	32.59	33.29	33.12	33.16	33.81
Efficiency	51.92	53.63	53.65	53.84	54.83
Relative head	1	1.0216	1.0163	1.0175	1.0376
Relative efficiency	1	1.0329	1.0333	1.0370	1.0560

The newly added dissipation term in the turbulent dissipation rate equation is given by Equation 3:

$$\frac{2\rho(1-F_1)}{\omega\sigma_{\omega 2}}\left(\frac{\partial k}{\partial x}\frac{\partial \omega}{\partial x}+\frac{\partial k}{\partial y}\frac{\partial \omega}{\partial y}+\frac{\partial k}{\partial z}\frac{\partial \omega}{\partial z}\right) \tag{3}$$

In the above equation, ρ is the density, G_k is the generation term of turbulent kinetic energy caused by the average velocity gradient, F_1 is the distance from the wall; $\sigma_{\omega 2}$, and β the constants, and are 5/9,0.075 and 2, respectively.

2.4 Boundary conditions

The working medium was set as a gas-liquid two-phase flow (comprising pure water and an ideal gas at a temperature of 25 °C). The liquid-phase turbulence model used was the *SST* $k-\omega$ model, and the gas-phase turbulence model adopted was the dispersed phase zero-equation model, with a bubble diameter of 0.1 mm. The inlet, guide blades, and outlet segments were modeled as stationary domains, whereas the impeller was modeled as a rotating domain. The inlet boundary condition was set as a velocity inlet with a velocity of 2.54 m/s, and the outlet was set as a pressure outlet with an outlet pressure of 3 MPa. The convergence criterion was based on the RMS method with a convergence accuracy of 10^{-5}. The rotational speed was set at 3,000 rpm. The wall boundaries were fixed under a no-slip condition, and a Scalable Wall Function was applied in the near-wall region.

The SIMPLE algorithm was used to solve the pressure and velocity. To ensure the stability of dynamic and static interfaces, the 'Frozen rotor' model was applied, and the static domains were handled using the General Grid Interface (GGI). The SIMPLE algorithm was employed for pressure-velocity coupling owing to its demonstrated robustness in handling complex rotational flows and gas-liquid two-phase systems characteristic of multiphase pumps. Whilst alternative algorithms such as SIMPLEC were also considered, preliminary tests indicated that SIMPLE exhibited superior convergence stability for the current configuration.

3 Multi-objective optimization framework

3.1 Optimization design process

The multi-objective optimal design system for blade multiphase pumps was constructed by integrating the Workbench and Isight platforms, enabling a closed-loop, full-process parametric design. In this system, the Workbench platform achieves forward-reverse hybrid design capability by modularly integrating the CFturbo reverse engineering module, turbogrid meshing module, ICEM CFD meshing module, and CFD simulation module. The CFturbo software integrated into the Workbench platform uses existing blade geometry data to reverse-engineer design parameters and generate fully parametric, editable models, facilitating the optimization of existing designs. He et al. (2021) Meanwhile, the Isight platform establishes an automated optimization decision chain via a multidisciplinary integrated interface, coupling CFD simulations, Design of Experiments (DOE), response surface approximation models (RSM), and various genetic algorithms. This approach effectively overcomes traditional iterative method bottlenecks, such as slow convergence (>50 cycles) and entrapment in local optima (Sun et al., 2018). Additionally, the platform includes a built-in convergence diagnostic module that terminates invalid iterations when design variables deviate from preset feasible domain thresholds during the generation of Pareto frontier solution sets, thereby conserving computational resources. The multiobjective optimization design platform for blade multiphase pumps is shown in Figure 3.

3.2 Optimization techniques

The optimization techniques used in the system include the DOE method, Response Surface Methodology (RSM), and various multi-objective optimization algorithms.

The DOE method, a key technique in mathematical statistics, is widely applied in product development and process optimization (Tian et al., 2023). For the blade multiphase pump booster unit, DOE provides sample points for approximate modeling and empirical formula construction. The Isight platform supports several DOE strategies: the Box-Behnken design, which uses three-level factor combinations to generate samples for quadratic response surface fitting; (He et al., 2025); the Latin hypercube design, which ensures global exploratory capacity through uniform sampling by random orthogonal combinations; (Rashid et al., 2019); and the Optimal Latin Hypercube Design (OLHD), which improves the homogeneity of Latin hypercube sampling, ensuring uniform distribution of test points across the design space. (Dash et al., 2020). In this study, OLHD is selected for sample generation due to its superior space-filling and balance properties, providing high-quality data for subsequent model training.

For optimization, this study employs the Nonlinear Constrained Genetic Algorithm (NCGA), which handles nonlinear constraints and performs efficient optimization in nonconvex feasible domains; (Zou et al., 2022); the multi-objective Particle Swarm Optimization (PSO) algorithm, which is known for its fast convergence in high-dimensional, discontinuous objective spaces, and the use of Pareto entropy weights for swarm intelligence-based searches (Guo and Abdul, 2021); and the Non-dominated Sorting Genetic Algorithm II (NSGA-II), which uses fast non-dominated sorting and crowding distance comparison operators to robustly filter multi-objective solution sets under complex constraint conditions (Li and Wang, 2021; Su et al., 2023; Zhou et al., 2023). The Pareto-optimal solutions obtained from these three algorithms are then validated using CFD numerical simulations to assess prediction error. The algorithm that

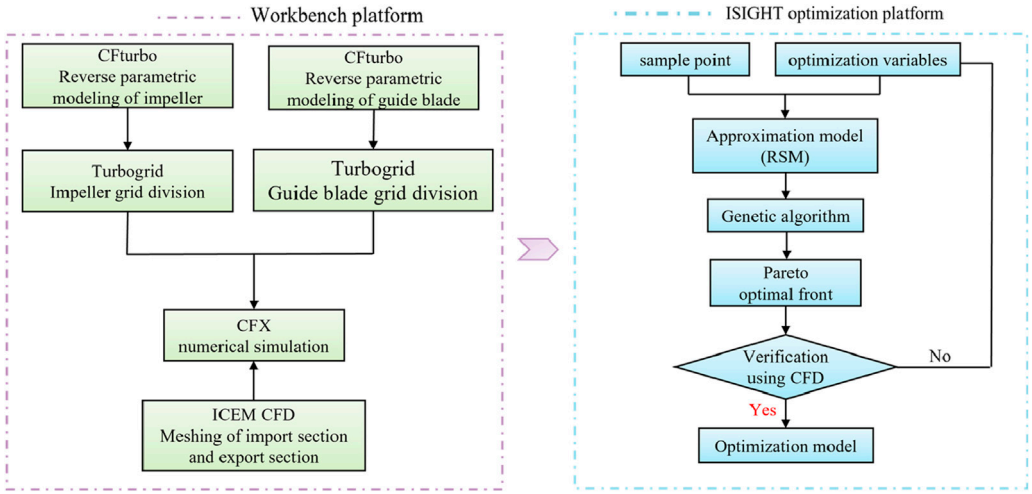

FIGURE 3
Multi-objective optimization design platform.

provides the richest solution set and the smallest error between the simulated and predicted values is ultimately selected to meet the multi-objective optimization needs of the blade multiphase pump under multiphase flow conditions.

4 Optimized parameter selection for the booster unit

4.1 Optimization variables

Based on the characteristics of the blade shape parameters of the booster unit of the blade multiphase pump and considering previous scholarly research (Zhang et al., 2017; Zhang et al., 2022a; Zhang et al., 2022b), the following are selected as optimization variables: the inlet angle at the hub of the impeller blade, the inlet angle at 50% blade height of the impeller blade, the inlet angle at the rim of the impeller blade, the half-cone angle of the impeller hub, the half-cone angle of the guide blade hub, and the impeller outlet wrap angle. Specifically, the inlet angle at the hub of the impeller blade was denoted as X_1, at 50% blade height as X_2, at the rim as X_3, the half-cone angle of the impeller hub as X_4, the half-cone angle of the guide blade hub as X_5, and the impeller outlet wrap angle as X_6. Because the inlet and outlet structures of the impeller and guide blade in the blade multiphase pump are symmetrical when optimal hydraulic performance is achieved, the half-cone angles of the impeller and guide blades (X_4 and X_5) are set to the same value. The optimization variable parameters and their corresponding ranges were determined based on design experience and are listed in Table 4. Figure 4 shows the meridian plane of the booster unit and its three-dimensional perspective view.

4.2 Optimization objective

According to the requirements for transport efficiency and stability of the transport medium during operation, the efficiency of the blade multiphase pump at 20% gas content and gas uniformity at the impeller outlet were selected as optimization objectives. The expression for the gas uniformity at the impeller outlet is given by Equation 4:

$$\sigma = \sqrt{\frac{\sum_{i=1}^{n}\left(\alpha_{g,i} - \overline{\alpha_g}\right)^2}{n-1}} \tag{4}$$

In the formula: $\overline{\alpha_g}$ is the average gas content, and $\alpha_{g,i}$ is the local air content The selected optimization goal is to achieve the highest possible efficiency of the blade multiphase pump at 20% gas content. The gas uniformity at the impeller outlet is closely related to the fluid pressure and velocity fields. A more uniform gas distribution, that is, a lower value, indicates a better flow state at the impeller outlet, which is conducive to the next stage of fluid transmission in the blade multiphase pump.

5 Parameter optimization results

5.1 Blade geometry parametric analysis

Based on the sensitivity analysis, the effects of the blade shape parameters on the efficiency and gas uniformity at the impeller outlet are shown in Figure 5. As can be seen:(1) The efficiency $\boldsymbol{\eta}$ shows a concave parabolic relationship with the inlet angle at the hub of the impeller blade X_1, while gas uniformity at the impeller outlet $\boldsymbol{\sigma}$ has a linear relationship with X_1 with a negative slope (Figure 5a). Specifically, as X_1 increased, the efficiency first decreased and then increased, whereas the gas uniformity continuously decreased. This indicates that an appropriate inlet angle at the hub improves the efficiency and reduces gas non-uniformity at the impeller outlet. (2) The efficiency $\boldsymbol{\eta}$ has a convex parabolic relationship with the inlet angle at 50% blade height X_2 and gas uniformity at the impeller outlet $\boldsymbol{\sigma}$ and gas uniformity shows a linear relationship with X_2 with a positive slope (Figure 5b). This result suggests that the efficiency can be improved with only a small increase in gas non-uniformity within a certain range of X_2, which

TABLE 4 Optimizing variable parameters and their ranges.

Blade shape parameters	X_1/°	X_2/°	X_3/°	X_4, X_5/°	X_6/°
Lower limit of a parameter	7.38	5.35	4.22	7.59	235
Upper limit of a parameter	9.00	6.53	5.14	14.93	250

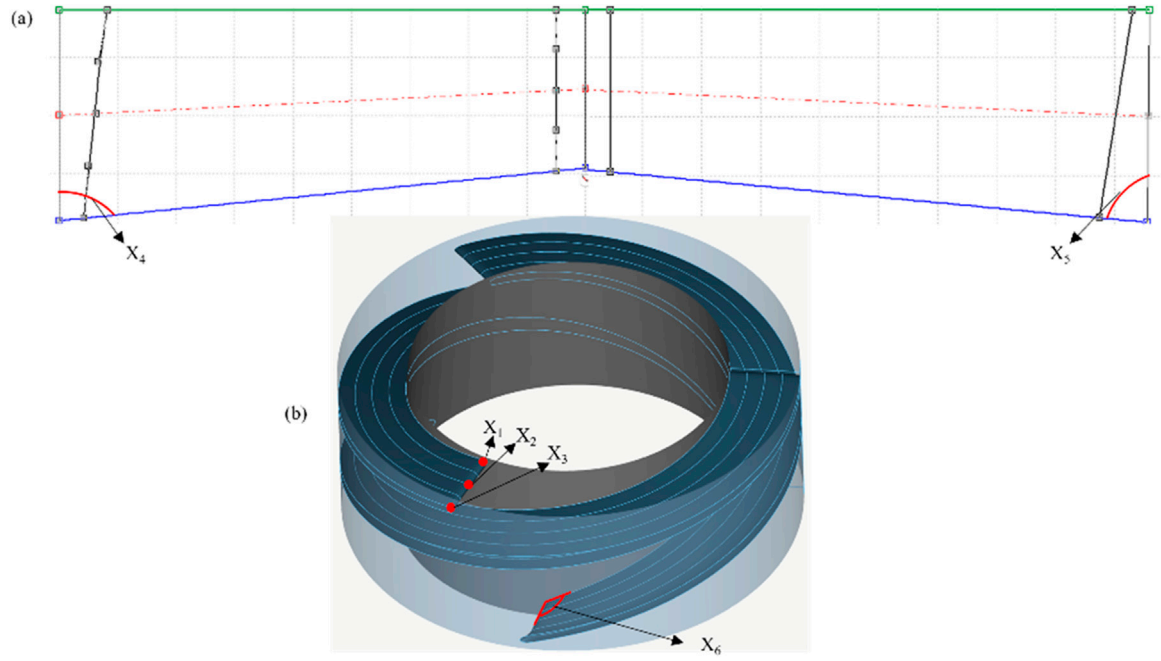

FIGURE 4
Geometric structure of booster unit. **(a)** Meridional plane, **(b)** 3D impeller.

should be considered when determining this angle. (3) As the inlet angle at the rim of the impeller blade X_3 increases, the efficiency $\boldsymbol{\eta}$ decreases slightly and then increases, while gas uniformity at the impeller outlet $\boldsymbol{c}$ behaves in the opposite manner (Figure 5c). This indicates that X_3 must be carefully selected to balance the efficiency and gas uniformity. (4) The effects of the half-cone angle of impeller hub X_4 and guide blade hub X_5 on the efficiency and gas uniformity at the impeller outlet were similar. Therefore, they were unified as the hub half-cone angle (X_4*) for analysis. Both efficiency $\boldsymbol{\eta}$ and gas uniformity at the impeller outlet $\boldsymbol{\sigma}$ have a linear relationship with X_4* with a negative slope. However, as X_4*increases, both efficiency and gas uniformity exhibit a strong overall decreasing linear trend. While minor non-monotonic fluctuations are present in the data for $\boldsymbol{\sigma}$, the dominant relationship is linear (Figure 4d, (e)). This suggests that selecting X_4* requires balancing efficiency and gas uniformity. (5) The impeller outlet wrap angle X_6 also affects efficiency $\boldsymbol{\eta}$ and the gas uniformity at the impeller outlet $\boldsymbol{\sigma}$ differently. As X_6 increases, the efficiency $\boldsymbol{\eta}$ shows a linear decrease, whereas the gas uniformity $\boldsymbol{\sigma}$ follows a convex parabolic trend (Figure 5f). This result suggests that selecting an appropriate X_6 can help reduce the number of optimization variables and save optimization time, while considering both efficiency and gas uniformity.

The contribution percentage of blade shape parameters to efficiency and gas uniformity at the impeller outlet is shown in Table 5. From Table 5, it can be seen that the impeller outlet wrap angle X_6 is the most significant influencing factor on both efficiency $\boldsymbol{\eta}$ and the gas uniformity at the impeller outlet $\boldsymbol{\sigma}$. Variations in X_6 directly and significantly affect the performance of the blade multiphase pump and the gas uniformity at the impeller outlet. The hub half-cone angle X_4* also has a significant influence on efficiency and gas uniformity. The size of the hub half-cone angle affects the shape of the flow path through the impeller and guide blades, which in turn affects the pump's ability to transport liquid and convert energy.

In contrast, the inlet angles at hub X_1, 50% leaf height X_2, and rim X_3 of the impeller blade, although they do have some effect on the efficiency and gas uniformity, have relatively smaller impacts. It is worth noting that the half-cone angle of the impeller hub plays a more prominent role in affecting efficiency than gas uniformity, while the inlet angle at 50% leaf height of the impeller blade appears to be more critical for optimizing efficiency.

In summary, the influence of each blade shape parameter on gas uniformity at the impeller outlet can be ranked as follows: impeller outlet wrap angle > hub half-cone angle > inlet angle at the rim of the impeller blade > inlet angle at 50% leaf height of the impeller blade > inlet angle at the hub of the impeller blade. The influence on efficiency can be ranked in the same order: impeller outlet wrap angle > hub half-cone angle > inlet angle at the rim of the impeller blade > inlet angle at 50% leaf height of the impeller blade > inlet

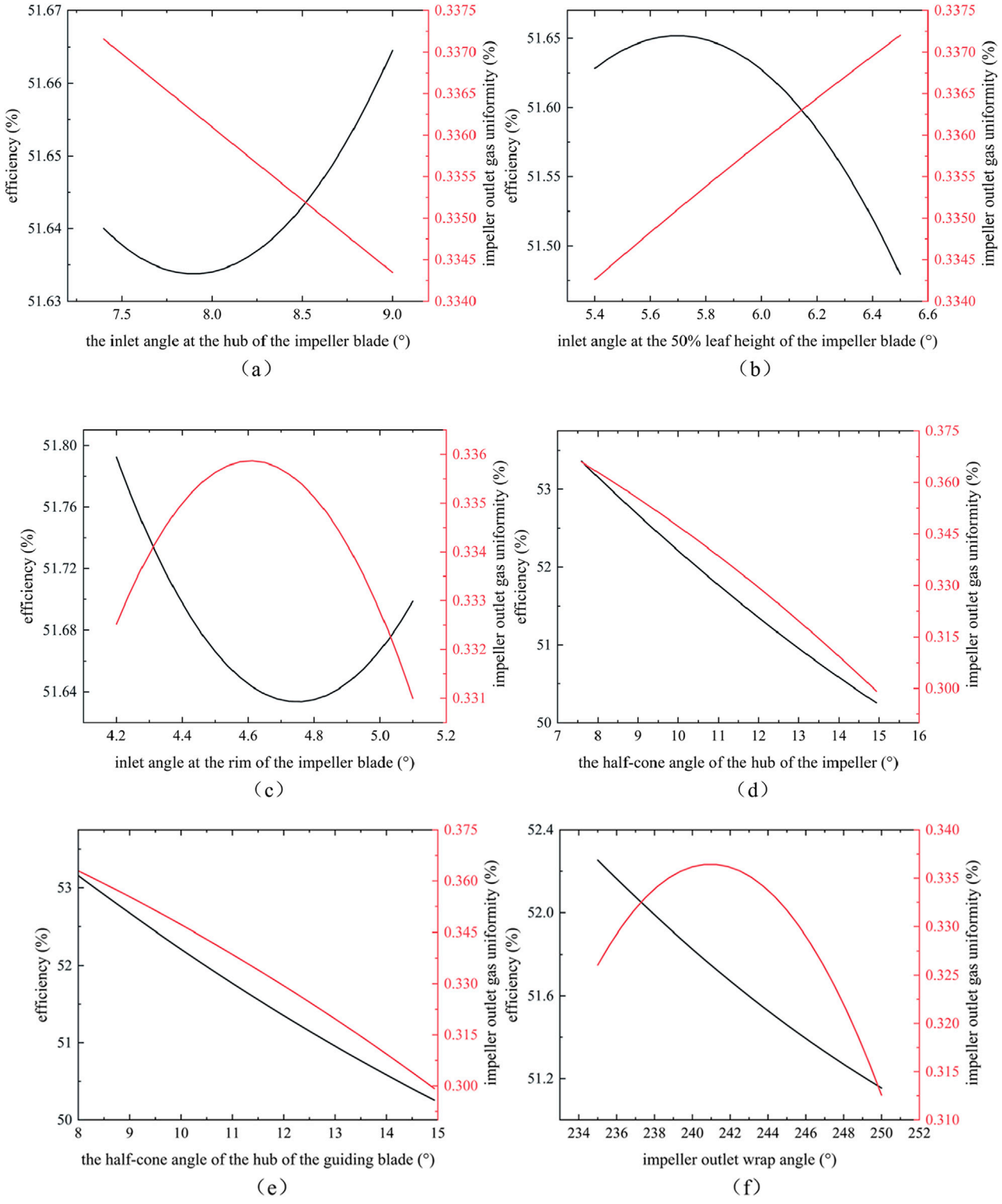

FIGURE 5
The influence of blade shape parameters on efficiency and gas uniformity at the impeller outlet. **(a)** the inlet angle at the hub of the impeller blade, **(b)** the inlet angle at the 50% leaf height of the impeller blade, **(c)** the inlet angle at the rim of the impeller blade, **(d)** the half-cone angle of the hub of the impeller, **(e)** the half-cone angle of the hub of the guiding blade, **(f)** the impeller outlet wrap angle.

TABLE 5 The contribution percentage of blade shape parameters to efficiency and gas uniformity at the impeller outlet.

Structural parameters	X_1	X_2	X_3	X_4*	X_6
Percentage contribution to efficiency/%	0.28	1.41	3.19	24.83	70.28
Percentage contribution to gas uniformity at the impeller outlet/%	2.71	2.75	2.98	15.47	76.08

angle at the hub of the impeller blade. These findings provide an important theoretical foundation and data support for the further optimization of blade multiphase pumps.

The main effects of blade shape parameters on the efficiency and gas uniformity at the impeller outlet are shown in Figure 6. As seen in Figure 6, the hub half-cone angle X_4* and the impeller outlet wrap angle X_6, as key influencing factors, have significant effects on both efficiency $\boldsymbol{\eta}$ and the gas uniformity at the impeller outlet $\boldsymbol{\sigma}$. The normalization method employed for the data in Figure 6 is the min-max normalization technique, its expression is given in Equation 5:

$$y_i = \frac{x_i - \min\limits_{1 \le i \le n}\{x_j\}}{\max\limits_{1 \le j \le n}\{x_j\} - \min\limits_{1 \le i \le n}\{x_j\}} \tag{5}$$

where $\boldsymbol{x_i}$ denotes the baseline sequence, $\boldsymbol{y_i}$ represents the new sequence, and $\boldsymbol{y_i} \epsilon (0, 1)$ is a dimensionless quantity.

Combining the results from Figures 5, 6, it can be concluded that there are significant differences in how each blade shape parameter affects efficiency and gas uniformity at the impeller outlet. Therefore, to effectively improve the efficiency while reducing gas non-uniformity, the interactions and independent effects of all blade shape parameters must be fully considered. An appropriate multi-objective optimization strategy should be adopted for decision analysis to determine the optimal combination of blade shape parameters to achieve the dual objectives of enhancing efficiency and controlling gas uniformity at the impeller outlet.

5.2 Approximate modelling

Given the complex nonlinear relationship between efficiency, gas uniformity at the impeller outlet, and the blade shape parameters, optimizing the booster unit parameters of a blade multiphase pump using a finite element model requires multiple cycles of 'design-test-improve-test. Therefore, in this study, a high-accuracy approximation model between the efficiency, gas uniformity at the impeller outlet, and each blade shape parameter was established to replace the finite element model within the design space.

This study employs RSM (Zhang et al., 2022a; Zhang et al., 2021), which can construct a smooth local response surface with fewer trials and uses mathematical methods to represent the relationship between input variables and output objectives. The minimum number of sample points required to construct the response surface approximation model, along with the mathematical expressions, is given as follows:

$$n_{min} = \frac{(M+1)(M+2)}{2} \tag{6}$$

$$\tilde{y} = \beta_0 + \sum_{i=1}^{k} \beta_i x_i + \sum_{i=1}^{k} \beta_i {x_i}^2 + \sum_{i \ne j} \beta_{ij} x_i x_j + \varepsilon \tag{7}$$

In the formula, M is the number of optimization variables, β_0 is a constant term, $\sum_{i=1}^{k} \beta_i x_i$ is the main effect term, $\sum_{i=1}^{k} \beta_i {x_i}^2$ is a non-linear effect term, $\sum_{i \ne j} \beta_{ij} x_i x_j$ is a variable synergy term, and ε is the random error.

From Equation 6, constructing a six-parameter full quadratic response surface model requires a minimum of $n_{min} = \frac{(6+1)(6+2)}{2} = 28$ sample points to avoid an underdetermined system. However, to enhance the model's accuracy, robustness, and space-filling coverage of the design domain, a larger sample size is warranted. Following established engineering practice for handling nonlinear systems and considering the need for reliable model validation, 90 sets of sample points were generated using the Optimal Latin Hypercube Design (OLHD). This sample size (approximately 3.2 times $\boldsymbol{n_{min}}$) provides a solid foundation for building a high-fidelity approximation model while maintaining computational efficiency. Based on the screened and pre-processed sample points, this study successfully established an approximate functional relationship between the efficiency of the booster unit of the blade multiphase pump and the gas uniformity at the impeller outlet as a function of the shape parameters of each blade. The specific functional polynomials are as follows.

$$\begin{aligned}\eta = {} & -419443.548769581 + 1702.04036042235X_1 \\ & + 1944.7373307466X_2 + 433.173680465094X_3 \\ & + 6775.8939600451X_4{}^* + 6775.89396600451X_6 \\ & -307.620090404544{X_1}^2 - 49.502997583543{X_2}^2 \\ & -131.707155187307{X_3}^2 - 41.7266154855006{X_4}^{*2} \\ & -2.00234365241493{X_6}^2 + 0.0494251972257435X_1X_2 \\ & + 0.05356777342187079X_1X_3 + 0.00363631301872415X_1X_4{}^* \\ & + 0.01095998325196127X_1X_6 - 0.40659255910749X_2X_3 \\ & -0.0164389208574212X_2X_4{}^* + 0.034174585103765X_2X_6 \\ & -0.0130295002055182X_3X_4{}^* + 0.0415822771815829X_3X_6 \\ & + 0.00243043159470906X_4{}^*X_6 + 24.6578022841042{X_1}^3 \\ & + 56.2070085161202{X_2}^3 + 17.913200204558{X_3}^3 \\ & + 0.114185514183185{X_4}^{*3} + 0.122731566238466{X_6}^3 \\ & -0.740316980554076{X_1}^4 - 2.39170956384184{X_2}^4 \\ & -0.910360339893269{X_3}^4 - 0.000117158134366879{X_4}^{*4} \\ & -0.00276689260392956{X_6}^4 \end{aligned} \tag{8}$$

TABLE 6 Fitting accuracy evaluation of the approximate model for efficiency and gas uniformity at the impeller outlet.

Fitting accuracy assessment metrics	Efficiency	Gas uniformity at the impeller outlet
Average (<0.2)	0.02741	0.04873
Maximum (<0.3)	0.22137	0.29533
Root mean square (<0.2)	0.04516	0.06673
R-squared (>0.9)	0.97218	0.92280

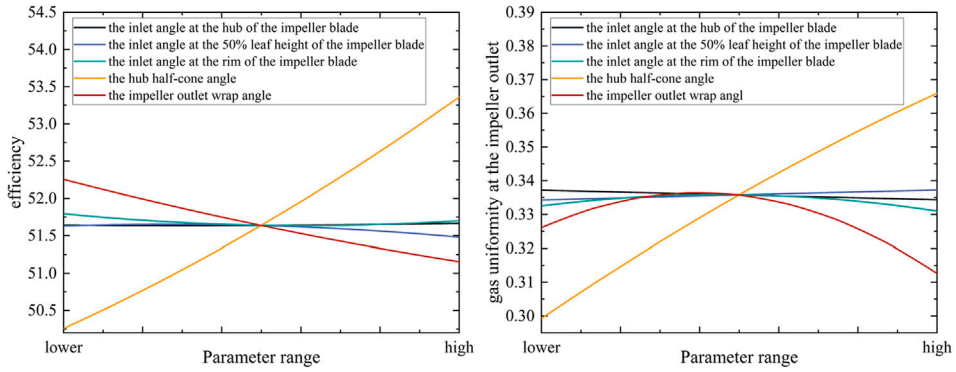

FIGURE 6
Main effect of the influence of blade shape parameters on efficiency and gas uniformity at the impeller outlet.

$$\begin{aligned}\sigma = {} & 25596.4541260554 - 35.325908885915X_1 \\ & + 36.5575013995594X_2 + 433.173680465094X_3 \\ & - 421.653178357846X_4{}^{*} - 0.219527257805638X_6 \\ & + 6.26522536695086{X_1}^2 - 8.92180368344{X_2}^2 \\ & -136.208681005368{X_3}^2 + 2.5965362396331{X_4}^{*2} \\ & + 0.023206402674207{X_6}^2 - 0.00483110159525789X_1X_2 \\ & -0.00139007402540168X_1X_3 - 0.00065894865065253X_1X_4{}^{*} \\ & + 0.000549739118401684X_1X_6 + 0.00205242842918737X_2X_3 \\ & + 0.000101679914401 69X_2X_4{}^{*} - 0.00146964857374443X_2X_6 \\ & + 0.000717342129413525X_3X_4{}^{*} - 0.0010271332723623X_3X_6 \\ & + 0.000265048548416794X_4{}^{*}X_6 - 0.490025597457608{X_1}^3 \\ & + 50.964992763110139{X_2}^3 + 3.7599342285805{X_3}^3 \\ & -0.00710456933790565{X_4}^{*3} - 0.0014956380296443{X_6}^3 \\ & + 0.01433692592995417{X_1}^4 - 0.0390005212550516{X_2}^4 \\ & -0.201959615835858{X_3}^4 - 7.28779922763096 \times 10^{-6}{X_4}^{*4} \\ & + 3.51257702066375 \times 10^{-5}{X_6}^4 \end{aligned} \quad (9)$$

While Equation 7 defines the standard second-order RSM, preliminary analysis indicated that a higher-order polynomial was necessary to adequately capture the complex nonlinear relationships between the blade parameters and the performance objectives. Therefore, the actual approximation models developed for efficiency (Equation 8) and gas uniformity (Equation 9) include third and fourth-order terms. This enhanced model form significantly improved the fitting accuracy, as validated by the metrics presented in Table 6. To evaluate the fitting accuracy of the approximation model built from the test sample points, the model was assessed using four types of accuracy metrics, as listed in Table 6. As shown in Table 6, the approximation model demonstrated high fitting accuracy for the test sample points.

To further validate the approximation model within the global constraint space, the residual sum of squares was analyzed in depth to evaluate its predictive performance for the relationship between the design variables and objective functions. Five sets of blade shape parameters from the test group were extracted to form the validation group. Their results, which were obtained by substituting into the approximation model, were compared with the finite element simulation results, as shown in Table 7.

The validation of the approximate model involved two complementary aspects. First, its global fitting accuracy was assessed using standard statistical metrics (R^2, RMSE, etc.) derived from the modeling procedure, as summarized in Table 6. The high R^2 values (>0.92) indicate the model reliably captures the overall design space trends. Second, and most critically for the optimization outcome, the model's predictive fidelity within the Pareto-optimal region was verified. Five representative design points, strategically selected to span the Pareto front obtained by the NCGA algorithm, were evaluated using high-fidelity CFD simulations. As shown in Table 7. At five key Pareto optimal points, the model predictions showed high consistency with CFD results: efficiency prediction error was 0.48% ± 0.12%, and gas uniformity prediction error was 3.23% ± 0.45%. The results demonstrate that the model exhibits excellent robustness and stability within the critical regions of interest for engineering decision-making. This two-pronged approach—global statistical assessment coupled with targeted verification at key Pareto-optimal points—effectively ensures the reliability of the model

TABLE 7 Comparison of the approximate model of efficiency and gas uniformity at the impeller outlet with the numerical simulation results.

Validation team	Blade shape parameters				
	X_1/°	X_2/°	X_3/°	X_4*/°	X_5/°
1	8.02	6.25	4.92	12.66	235.00
2	8.76	6.52	4.98	12.50	242.58
3	8.04	5.36	4.94	11.19	238.71
4	7.84	6.45	5.08	12.01	241.57
5	7.53	6.07	4.27	8.77	245.28
Approximate modelled value of efficiency/%	Numerical simulation value of efficiency/%	Relative deviation of the two/%	Approximate modelled value of gas uniformity at the impeller outlet	Numerical simulation value of gas uniformity at the impeller outlet	Relative deviation of the two/%
51.581	51.566	0.039	54.56	0.315	1.378
51.238	50.785	0.890	51.81	0.325	1.421
52.002	52.004	0.003	53.83	0.324	1.213
51.497	51.205	0.570	51.79	0.326	0.995
52.671	52.736	0.124	53.80	0.353	0.900

predictions where it matters most for the final design, while remaining computationally feasible.

5.3 Optimization mathematical modelling

Based on the parametric analysis and the established approximate models, a multi-objective optimization mathematical model is formulated to systematically determine the optimal blade geometry. The model is defined by the design variables, objective functions, and constraints, as detailed below.

The design variables are the six key blade shape parameters previously defined:

$$X = [X_1, X_2, X_3, X_4.X_5, X_6]^T \tag{10}$$

In the Equation 10, X denotes the vector consisting of the design variables; $F_{obj}(X_1, X_2, X_3, X_4.X_5, X_6)$ is the objective function for multi-objective optimal design, the feasible ranges for these variables are constrained according to Table 4.

The optimization aims to simultaneously maximize the pump efficiency ($\boldsymbol{\eta}$) at 20% gas content and minimize the gas uniformity coefficient ($\boldsymbol{\sigma}$) at the impeller outlet. These two objectives often conflict with each other; thus, the goal is to find a set of Pareto-optimal solutions that represent the best possible compromises.

The corresponding multi-objective optimization problem is formulated as follows:

$$F_{obj1}(X) = \eta(X) \tag{11}$$

$$F_{obj2}(X) = \sigma(X) \tag{12}$$

$$X_{i,min} \le X_i \le X_{i,max}, i = 1, 2, 3 \ldots, 6 \tag{13}$$

In the Equations 11–13, $\boldsymbol{\eta}(\boldsymbol{X})$ and $\boldsymbol{\sigma}(\boldsymbol{X})$ the Response Surface Methodology (RSM) given by Equations 8, 9, which approximate the pump's performance based on the blade shape parameters. The constraints ensure that the optimal solution resides within the pre-defined practical design space.

5.4 Optimal parameter selection

5.4.1 Algorithm configuration

In the optimization process, the response relationship between the optimization variables and objectives was determined using the numerical results from 90 sets of sample points, allowing the construction of an approximate model linking the variables and objectives. In this study, to effectively search for the optimal blade shape parameters within the global design space, three global optimization algorithms are employed: the Nonlinear Constrained Genetic Algorithm (NCGA), Multi-Objective Particle Swarm Optimization algorithm (Multi-Objective Particle Swarm), and Non-dominated Sorting Genetic Algorithm II (NSGA-II). These algorithms were used to explore the efficiency of the blade multiphase pump and gas uniformity at the impeller outlet within the defined feasible domains. The specific configurations of these optimization algorithms are as follows:

The Nonlinear constrained genetic algorithm (NCGA) had a population size of 20, 40 generations, crossover type of 1, crossover rate of 0.01, and 801 iterations. Multi-Objective Particle Swarm optimization algorithm (Multi-Objective Particle Swarm): The maximum number of iterations was 24, the number of particles was 34, the inertia was 0.9, the maximum velocity was 0.1, and the number of iterations was 816. The non-dominated sorting genetic algorithm (NSGA-II) has a population size of 24, number of generations of 34, crossover probability of 0.9, and number of iterations of 816.

TABLE 8 Optimization results of multi-objective optimization algorithm.

Optimization algorithm	Efficiency	Impeller outlet gas uniformity	Number of pareto optimal solutions	Number of iterations
Nonlinear constrained genetic algorithm (NCGA)	53.686	0.2945	192	801
Multi-objective particle swarm optimization algorithm (Multi-Objective Particle Swarm)	53.242	0.3103	7	1,001
Non-dominated sorting genetic algorithm (NSGA-II)	53.739	0.3092	27	401

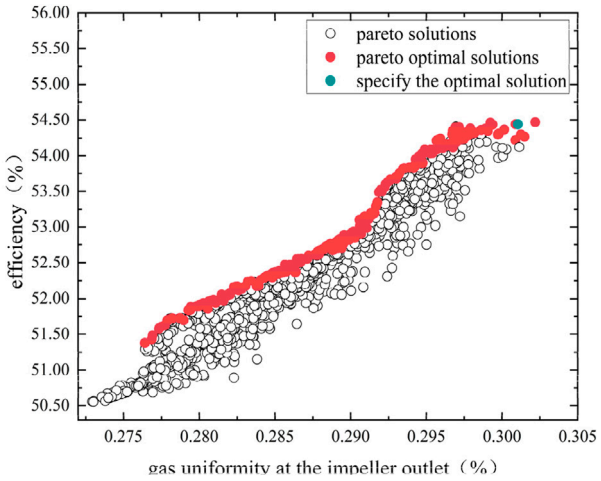

FIGURE 7
Optimized solution set.

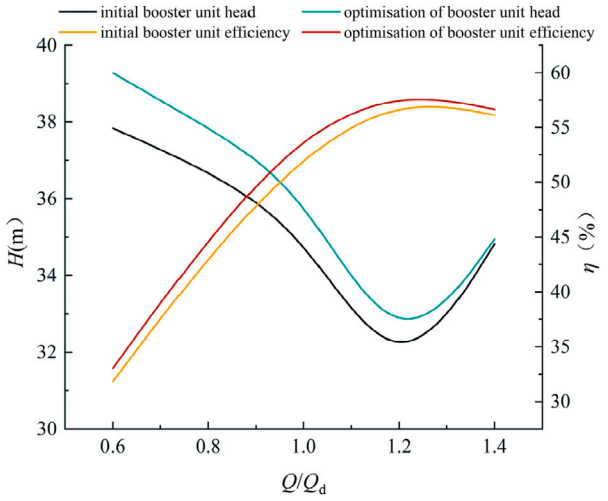

FIGURE 8
Comparison of blade multiphase pump hydraulic characteristic curves before and after optimization.

5.5 Optimal outcome

These three multi-objective optimization algorithms perform global searches within the defined feasible domain. The values and numbers of the Pareto optimal solutions obtained are listed in Table 8. To statistically validate performance differences, each algorithm underwent five independent runs. NCGA consistently demonstrated superior performance, with a standard deviation of 0.012, significantly outperforming both MOPSO (standard deviation: 0.018) and NSGA-II (standard deviation: 0.015). According to the Wilcoxon signed-rank test ($p < 0.05$), this indicates that NCGA's superiority is statistically significant and not attributable to chance. Comparative evaluation reveals trade-offs in performance: the NCGA algorithm achieves the highest-quality Pareto optimal solutions and demonstrates superior computational efficiency, making it the preferred choice when solution quality is the primary objective. However, the NSGA-II algorithm exhibits faster initial convergence rates, making it an attractive alternative for applications requiring rapid acquisition of high-quality solutions. Consequently, algorithm selection should be determined by the specific priorities of the optimization task—whether pursuing ultimate performance or prioritizing efficiency. In this optimization design, both ultimate performance and computational efficiency are required, hence the NCGA algorithm is selected as the optimization algorithm for this instance.

As shown in Table 8, the NCGA demonstrated the best performance in the global optimization process. It produced the richest set of Pareto optimal solutions, achieved the highest efficiency under the optimized blade shape parameters, and yielded the lowest gas uniformity at the impeller outlet. Therefore, the blade shape parameters identified by the NCGA were selected as the optimal solutions in this study. Figure 7 Pareto-optimal solution set for the NCGA algorithm While the Pareto front of NCGA is visualized in Figure 7, the quantitative superiority of its solution set over those of MOPSO and NSGA-II is conclusively established by the metrics in Table 8.

Figure 7 illustrates the pareto-optimal solution set for the NCGA algorithm. The optimal solution selected by the NCGA algorithm is used as the final result, and the corresponding optimal blade shape parameters are as follows: the inlet angle at the hub of the impeller blade: 8.36°, the inlet angle at the 50% leaf height of the impeller blade: 6.12°, the inlet angle at the rim of the impeller blade: 4.57°, the half-cone angle of the impeller hub: 7.59°, the half-cone angle of the guide blade hub: 7.59°, the impeller outlet wrap angle: 241.07°. By comparing the target optimized and simulated values of the efficiency and gas uniformity at the impeller outlet after blade shape parameter optimization, the errors were found to be 0.48% and 3.23%, respectively, both within acceptable tolerances, confirming the reliability of the optimization results. Furthermore, compared to the prototype blade multiphase pump, the optimized parameters increased the efficiency from 52.60% to 54.56% (an improvement of 3.59%) and reduced the gas uniformity

TABLE 9 Hydraulic loss before and after optimization.

Pump type	/(%)	Losses in the inlet section/%	Losses in the impeller section/%	Losses in the glade blade section/%	Losses in the outlet section/%
Prototype pumps	52.60	4.07	15.87	12.685	11.05
Optimized pumps	54.56	3.19	13.50	11.05	5.34

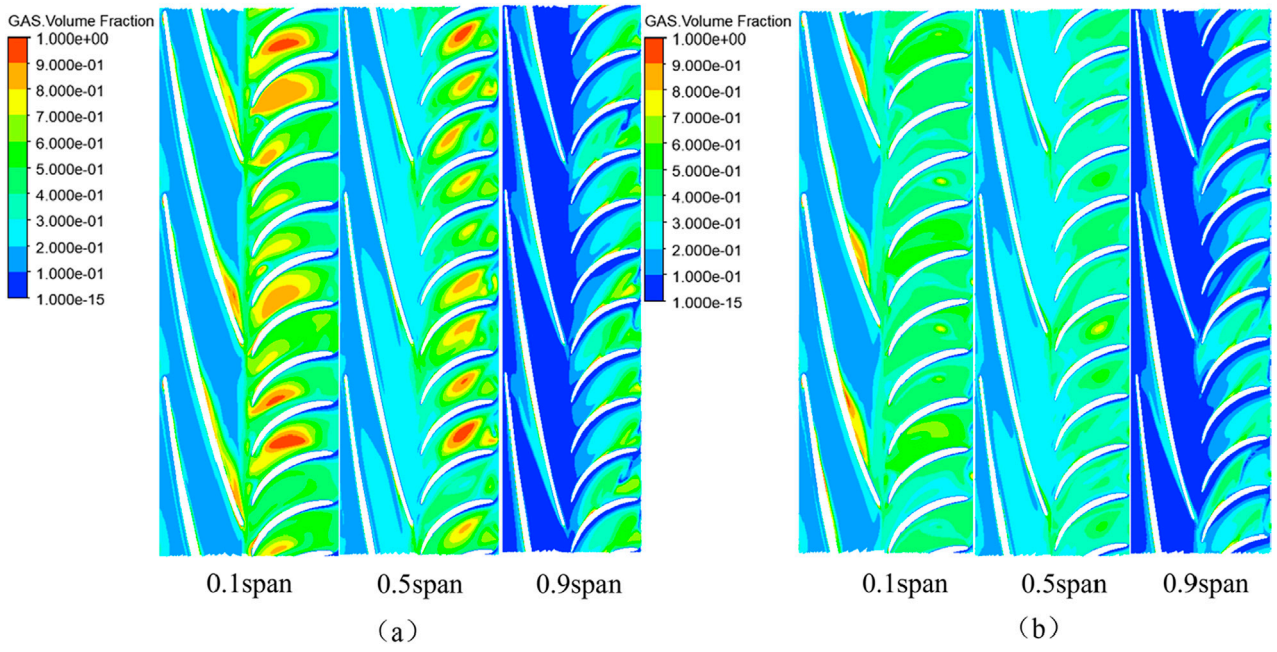

FIGURE 9
The distribution of gas void fraction at different blade span of the booster unit **(a)** before and **(b)** after optimization.

at the impeller outlet from 0.3229 to 0.3040 (a decrease of 6.22%). This demonstrates the significance of parameter optimization in improving the pump efficiency and reducing gas non-uniformity.

6 Optimization results analysis

6.1 Comparative analysis of external characteristics

The hydraulic characteristic curves of the blade multiphase pump before and after optimization are compared in Figure 8. As shown in Figure 8, the hydraulic efficiency and head of the optimized pump are improved across the operating range of 0.6Q to 1.4Q. The hydraulic efficiency improvements at 0.6*Q*, 0.8*Q*, 1.0*Q*, 1.2*Q*, and 1.4*Q* were 3.64, 3.68, 3.57, 1.02, and 0.90%, respectively. The corresponding head improvements under these conditions are 3.68%, 2.95%, 2.97%, 2.02%, and 0.37%, respectively. From the perspective of hydraulic efficiency and head enhancement under varying working conditions, the optimization significantly improves the pump's hydraulic performance at lower flow rates, supporting the adaptability of multiphase mixing pumps under small-flow conditions.

To further compare the hydraulic loss changes of the blade multiphase pump optimized using the NCGA algorithm with those of the original model pump, the changes in the efficiency and hydraulic losses in each section of the pump before and after optimization were examined. The results are presented in Table 9.

A comparison of the losses in each section of the pump before and after optimization showed a significant reduction in hydraulic losses. The adjustment of the blade parameters in the booster unit reduces local losses at the impeller and guide blade and minimizes the local loss caused by the flow impact at the junction between the inlet section and impeller. However, owing to the presence of vortices and velocity loops on the outlet side of the guide blade, a certain amount of hydraulic loss remained in the outlet section.

6.2 Comparative analysis of internal flow fields

The analysis also compares the distribution of the gas void fraction at different blade spans of the booster unit before and after optimization, as shown in Figure 9. From Figure 9, it can be observed that at 0.1 span, there is evident flow separation in the

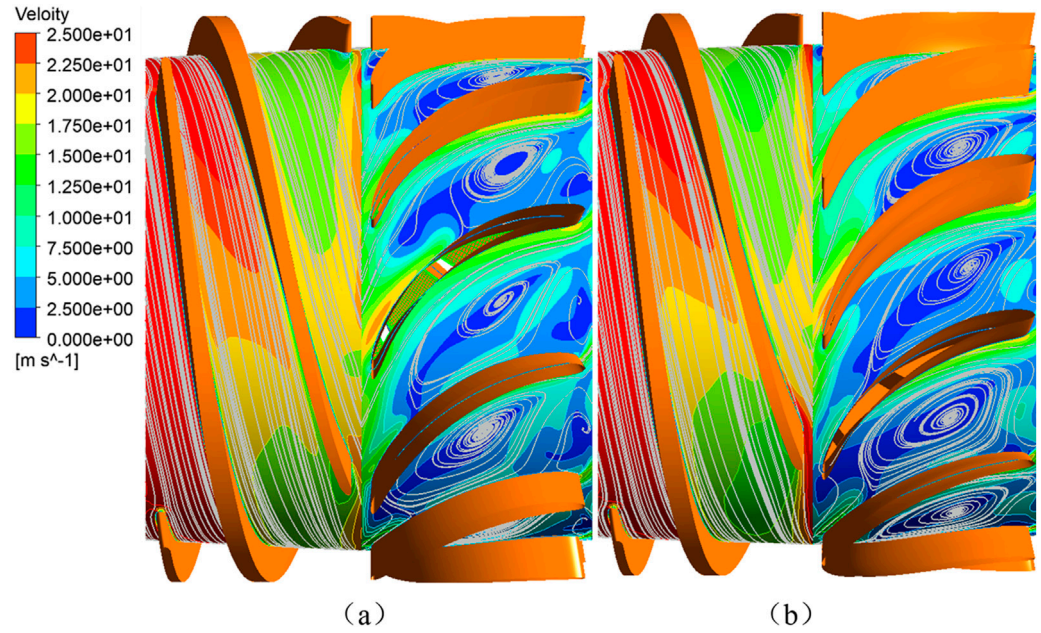

FIGURE 10
Velocity and streamline patterns of the booster unit **(a)** before and **(b)** after optimization (0.5span).

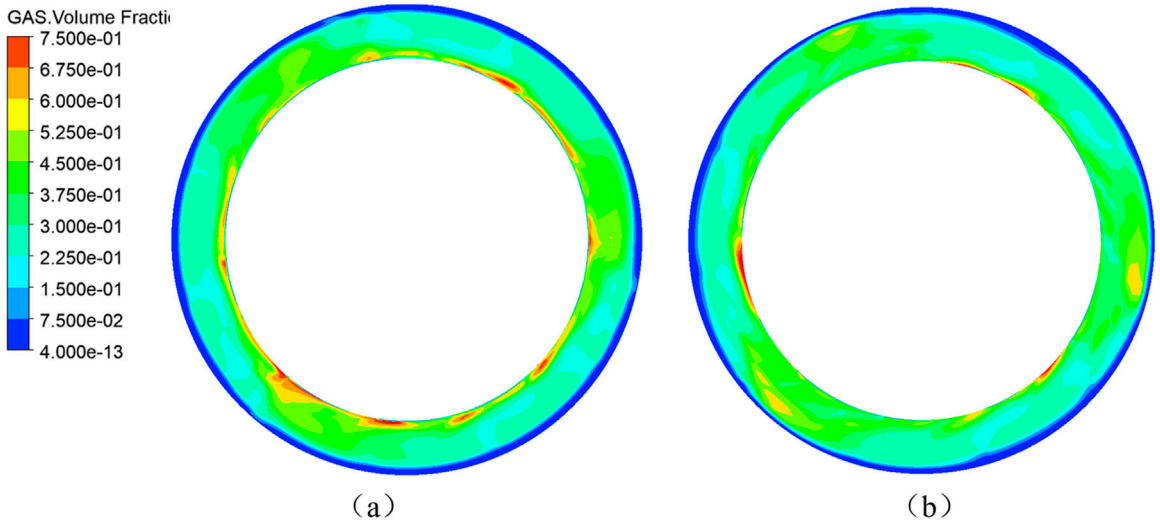

FIGURE 11
Gas uniformity at the impeller outlet **(a)** before and **(b)** after optimization.

pre-optimization booster unit, with a localized region of high gas content at the impeller outlet and guide blade inlet. After optimization, the gas-liquid two-phase distribution in the booster unit became more uniform, wall boundary layer separation was suppressed, and the extent of the high gas content region was significantly reduced. At a span of 0.5, most of the gas in the pre-optimization booster unit was concentrated in the middle and rear parts of the guide blade passage, with a localized high gas-content zone. After optimization, the uniformity of the gas distribution in the flow path of the booster unit improved significantly, and the local high gas content region was eliminated, enhancing the energy transfer efficiency. At 0.9 span, the gas in the pre-optimization booster unit is mainly located at the guide blade outlet. After optimization, the gas-liquid mixing becomes more balanced, and the gas content at the guide blade outlet decreases, reducing the risk of gas plugging during transportation.

The velocity and streamline patterns of the booster unit at 0.5 span before and after optimization are compared in Figure 10. Figure 10 shows that velocity variations within the

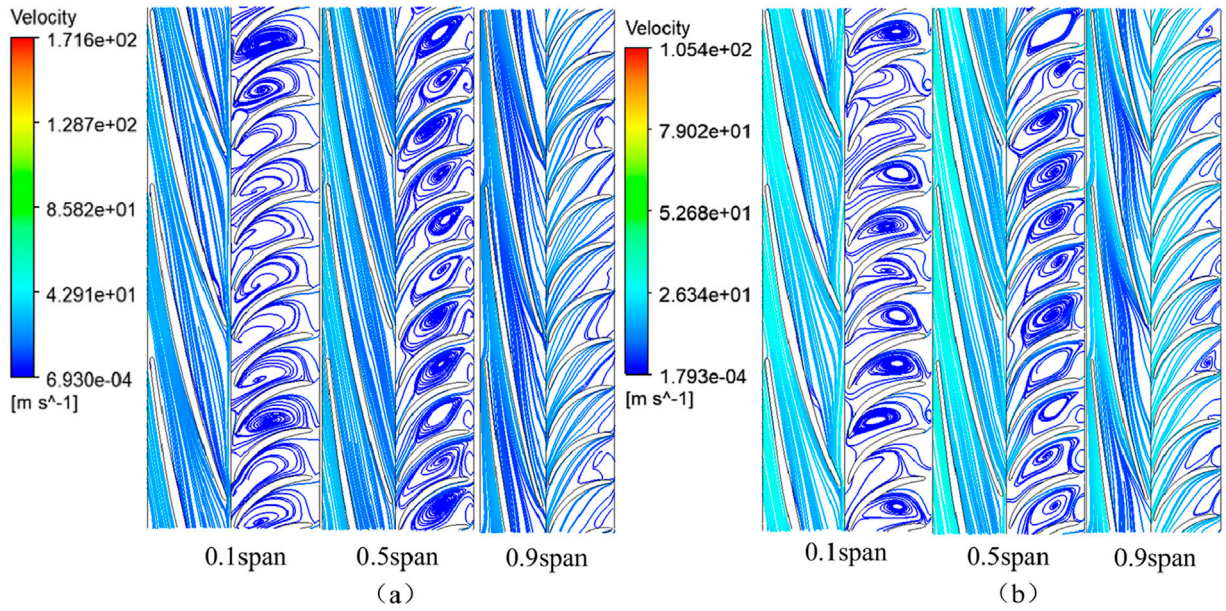

FIGURE 12
The Streamline patterns at different blade span of the booster unit **(a)** before and **(b)** after optimization.

impeller were not pronounced before optimization, whereas strong vortex formations were present in the guide blade flow channel, increasing the flow energy dissipation. After optimization, the low-velocity region within the guide blade was reduced.

The gas uniformity at the impeller outlet before and after the optimization is compared in Figure 11. As shown in Figure 11, prior to optimization, a band of high gas content was distributed circumferentially at the impeller outlet, with a prominent high gas-content region near the hub. After optimization, the gas content distribution became significantly more uniform, and the high-gas region near the hub was reduced. This indicates improved gas uniformity in the booster unit and enhanced mixing capability of the pump after optimization.

The streamline patterns at different blade spans of the booster unit before and after optimization are compared in Figure 12. From Figure 12, it can be observed that at 0.1 span, flow separation occurs near the hub wall in the pre-optimization booster unit owing to streamline detachment, resulting in local energy dissipation. This separation region was reduced after optimization. At a span of 0.5, the pre-optimization booster unit shows a low-speed stagnation zone, hindering effective gas-liquid mixing. After optimization, the vortex region was diminished, and the gas-liquid mixing efficiency was significantly improved. At 0.9 span, the changes before and after optimization were not substantial, primarily because the liquid phase dominated near the rim.

Although the optimal geometric parameters derived in this study are based on a specific type of multiphase pump with its operating conditions, the optimization framework itself possesses good generalizability and can be extended for application in the design of other turbomachinery. Subsequent research may further validate the applicability of this framework across different pump types and operating conditions, with the aim of establishing more universally applicable design principles for multiphase pumps.

While the current optimization achieved a balanced improvement in hydraulic efficiency and gas uniformity capability, further performance gains could be explored in future work. Potential strategies include expanding the geometric design space to include parameters like blade lean and sweep, employing high-fidelity transient turbulence models to better resolve complex flow structures, utilizing three-dimensional free-form deformation for more radical blade redesign, and performing system-level optimization for stability across multiple operating conditions.

7 Conclusion

This study establishes an integrated multi-objective optimization framework for a multiphase pump booster unit. The methodology combines three-dimensional inverse design, computational fluid dynamics (CFD) simulation, response surface methodology (RSM), and genetic algorithms. The principal findings may be summarized as follows:

The half-cone angle and the impeller outlet wrap angle have been identified as the most significant geometric parameters influencing pump efficiency and gas uniformity at the impeller outlet.

Among various comparison algorithms, the Non-Dominated Sorting Genetic Algorithm (NCGA) demonstrates the most effective performance in generating a richly diverse set of Pareto optimal solutions.

The optimized booster unit design delivers multiple performance enhancements: efficiency increases from 52.60% to 54.56% (a relative improvement of 3.59%), while gas uniformity at the impeller outlet decreases from 0.3229 to 0.3040 (a reduction of 6.22%). Analysis of

both external characteristics and internal flow fields further confirms that the optimized design effectively enhances hydraulic performance and promotes more uniform gas-liquid dispersion.

In summary, the proposed RSM-NCGA collaborative optimization strategy provides a systematic and effective solution for performance-driven design of multiphase pumps, demonstrating promising prospects for industrial application.

Data availability statement

The original contributions presented in the study are included in the article/Supplementary Material, further inquiries can be directed to the corresponding authors.

Author contributions

PD: Conceptualization, Data curation, Formal Analysis, Investigation, Methodology, Software, Validation, Writing – original draft. GS: Conceptualization, Formal Analysis, Funding acquisition, Methodology, Supervision, Writing – review and editing. YX: Conceptualization, Project administration, Software, Supervision, Writing – review and editing. HW: Conceptualization, Project administration, Software, Supervision, Writing – review and editing. WL: Conceptualization, Project administration, Software, Supervision, Writing – review and editing. XP: Conceptualization, Project administration, Software, Supervision, Writing – review and editing.

Funding

The author(s) declared that financial support was received for this work and/or its publication. This research was funded by the Sichuan Natural Science Foundation Outstanding Youth Science Foundation (2024NSFJQ0012), the Key Project of Regional Innovation and Development Joint Fund of the National Natural Science Foundation (U23A20669), the Sichuan Science and Technology Program (2022ZDZX0041), the Open Research Subject of Key Laboratory of Fluid and Power Machinery (Xihua University), and the Ministry of Education–Research on Cavitation Mechanism of Hydraulic Impactor (LTDL-2023001).

Conflict of interest

The author(s) declared that this work was conducted in the absence of any commercial or financial relationships that could be construed as a potential conflict of interest.

Generative AI statement

The author(s) declared that generative AI was not used in the creation of this manuscript.

Any alternative text (alt text) provided alongside figures in this article has been generated by Frontiers with the support of artificial intelligence and reasonable efforts have been made to ensure accuracy, including review by the authors wherever possible. If you identify any issues, please contact us.

Publisher's note

References

Chen, L., Yang, Y. X., Song, X., Zhang, X. D., and Gong, Y. (2024). Integrated optimization design of multiphase pump based on adaptive sparse grid method. *Ocean. Eng.* 298, 117235. doi:10.1016/j.oceaneng.2024.117235

Dash, S., Mandal, B. N., and Parsad, R. (2020). On the construction of nested orthogonal Latin hypercube designs. *Metrika* 83 (3), 347–353. doi:10.1007/s00184-019-00721-w

Ge, Z. G., Luo, X. Q., Feng, J. J., Zhu, G. J., He, D. H., and Wu, G. K. (2023). Multi-objective and multi-condition optimization for a gas–liquid mixed-flow pump based on a three-dimensional inverse design. *Phys. Fluids* 35 (6). doi:10.1063/5.0156054

Gu, Z. Y., Zhang, J. T., Zhang, W., and Wei, Y. K. (2025). A multi-objective aerodynamic performance optimization of a centrifugal vacuum pump and the flow physics analysis. *AIP Adv.* 15 (4), 045324. doi:10.1063/5.0268993

Guo, L. P., and Abdul, N. M. M. (2021). Design and evaluation of fuzzy adaptive particle swarm optimization based maximum power point tracking on photovoltaic system under partial shading conditions. *Front. Energy Res.* 9, 712175. doi:10.3389/fenrg.2021.712175

Han, W., Yang, S. Q., Li, R. N., Tian, Y. P., and Yang, T. (2024a). Coupled effects of hub diameter ratio and blade angle on the performance of spiral axial flow gas liquid multiphase pump. *J. Appl. Fluid Mech.* 17 (10), 2154–2168. doi:10.47176/jafm.17.10.2622

Han, W., Zhou, J. P., Li, R. N., Ma, X. N., and HaojieWang, (2024b). Influence of trailing edge flap length and deflection angle on the performance of the multiphase pump. *P I Mech. Eng. A-J Pow.* 238 (3), 457–468. doi:10.1177/09576509231211395

He, D. H., Li, R. L., Zhang, Z. D., Sun, S. H., and Guo, P. C. (2021). Gas–liquid two-phase flow pattern identification of a centrifugal pump based on SMOTE and artificial neural network. *Micromachines* 13 (1), 2. doi:10.3390/mi13010002

He, F., Zheng, X., Luo, W., Zhong, J., Huang, Y., Ye, A., et al. (2025). Collaborative optimization of aerodynamics and wind turbine blades. *Appl. Sci.* 15 (2), 834. doi:10.3390/app15020834

Li, B., and Wang, J. W. (2021). Economic dispatch methods for smart grid based on improved SPEA2 and improved NSGA2. *Front. Energy Res.* 9, 767721. doi:10.3389/fenrg.2021.767721

Li, C. H., Luo, X. Q., Feng, J. J., Zhu, G. J., and Yan, S. N. (2020). Effect of diversion cavity geometry on the performance of gas-liquid two-phase mixed transport pump. *Energies* 13 (8), 1882. doi:10.3390/en13081882

Lirong, D. O., Zhixin, W. E., Jianjun, W. A., Zhaoming, W. A., Zhengjun, H. E., and Xiaobing, L. I. (2022). Analysis of the world oil and gas exploration situation in 2021. *Petrol Explor Dev.* 49 (5), 1033–1044. doi:10.11698/PED.20220160

Liu, M., Tan, L., and Cao, S. L. (2018). Design method of controllable blade angle and orthogonal optimization of pressure rise for a multiphase pump. *Energies* 11 (5), 1048. doi:10.3390/en11051048

Liu, M., Tan, L., Xu, Y., and Cao, S. L. (2020). Optimization design method of multi-stage multiphase pump based on oseen vortex. *J. Petrol Sci. Eng.* 184, 106532. doi:10.1016/j.petrol.2019.106532

Longxin, M., and Zhifeng, J. (2019). Technological progress and development directions of PetroChina overseas oil and gas exploration. *Petrol Explor Dev.* 46 (6), 1088–1099. doi:10.1016/S1876-3804(19)60265-X

Peng, C. C., Zhang, X. D., Chen, Y. Q., Gong, Y., Li, H. D., and Huang, S. X. (2022a). A method for the integrated optimal design of multiphase pump based on the sparse grid model. *Processes* 10 (7), 1317. doi:10.3390/pr10071317

Peng, C. C., Xiaodong, Z., Zhiguang, G., Ju, W., and Yan, G. (2022b). Research on cooperative optimization of multiphase pump impeller and diffuser based on adaptive refined response surface method. *Adv. Mech. Eng.* 14 (1), 16878140211072944. doi:10.1177/16878140211072944

Rashid, F., Akbar, A., and Zafar, Z. (2019). Some new third order designs robust to one missing observation. *Commun. Stat. Theory Methods* 48 (24), 6054–6062. doi:10.1080/03610926.2018.1528362

Shi, G. T., Li, H. L., Liu, X. B., Liu, Z. K., and Wang, B. N. (2021). Transport performance improvement of a multiphase pump for gas–liquid mixture based on the orthogonal test method. *Processes* 9 (8), 1402. doi:10.3390/pr9081402

Su, R., He, G. B., Su, S., Duan, Y. R., Cheng, J. Z., Chen, H., et al. (2023). Optimal placement and capacity sizing of energy storage systems via NSGA-II in active distribution network. *Front. Energy Res.* 10, 1073194. doi:10.3389/fenrg.2022.1073194

Suh, J. W., Kim, J. W., Choi, Y. S., Kim, J. H., Joo, W. G., and Lee, K. Y. (2017). Multi-objective optimization of the hydrodynamic performance of the second stage of a multiphase pump. *Energies* 10 (9), 1334. doi:10.3390/en10091334

Sun, P., Wang, X. L., and Xie, W. C. (2018). Centrifugal blower of stratospheric airship. *IEEE Access* 6, 10520–10529. doi:10.1109/ACCESS.2018.2809707

Tang, W., Shi, G. T., Xiao, Y. X., Huang, Z. L., Li, W., and Chen, W. X. (2023). Study on the blade squealer tip affecting tip leakage flow and performance of a multiphase pump. *Phys. Fluids* 35 (2), 025137. doi:10.1063/5.0140688

Tian, F., Yang, C., Zhang, E. R., Sun, D. H., Shi, W. D., and Chen, Y. H. (2023). Design optimization of hydraulic machinery based on ISIGHT software: a review of methods and applications. *Water* 15 (11), 2100. doi:10.3390/w15112100

Wang, J. Q., Hu, C., Bai, L., Agarwal, R., Agarwal, R., and Zhou, L. (2024). Effect of the impeller blade outlet setting angle on the performance of the helical axial-flow multiphase pump. *Front. Energy Res.* 12, 1364955. doi:10.3389/fenrg.2024.1364955

Wen, H. G., Lv, W. J., Shi, G. T., and Liu, Z. K. (2022). Effect of the tip clearance on tip leakage vortex and pressure fluctuation characteristics in a helico-axial flow multiphase pump. *AIP Adv.* 12 (8), 085326. doi:10.1063/5.0096600

You, L., and Peng, C. C. (2023). Effect of variable speed conditions on the internal flow characteristics of a multiphase pump. *Chem. Eng. Res. Des.* 199, 348–362. doi:10.1016/j.cherd.2023.09.028

Zhang, J. Y., Cai, S. J., Li, Y. J., Zhou, X., and Zhang, Y. X. (2017). Optimization design of multiphase pump impeller based on combined genetic algorithm and boundary vortex flux diagnosis. *J. Hydrodyn.* 29 (6), 1023–1034. doi:10.1016/S1001-6058(16)60816-8

Zhang, R. H., Gao, L. D., and Chen, X. B. (2021). Optimization design of centrifugal pump impeller based on multi-output Gaussian process regression. *Mod. Phys. Lett. B* 35 (21), 2150364. doi:10.1142/S0217984921503644

Zhang, W., Zhu, B. S., Zi, D., Ma, Z., and Wang, F. J. (2022a). Transportability improvement of a gas–liquid rotodynamic pump using the two-step multi-objective optimization strategy. *Front. Energy Res.* 10, 900182. doi:10.3389/fenrg.2022.900182

Zhang, W., Zhu, B., Wang, Z., and Wang, F. (2022b). Optimization design for an impeller of the multiphase rotodynamic pump handling gas-liquid two-phase flow. *P I Mech. Eng. A-J Pow.* 236 (8), 1544–1557. doi:10.1177/09576509221098223

Zhou, S. Q., Zhang, T. L., Mao, Z. J., and Liu, Y. F. (2023). Multi-objective optimization of an IGV for a large axial fan based on NSGA-II. *Front. Energy Res.* 10, 994654. doi:10.3389/fenrg.2022.994654

Zhou, H. Z., Chun, X., Zhou, P., Zhou, P. J., Wu, Y. Z., Meng, L., et al. (2024). Numerical simulation study of vortex cavitation and induced pulsation characteristics in spiral lobe pumps. *AIP Adv.* 14 (12), 125311. doi:10.1063/5.0238468

Zou, D. H., Fan, Y., Liu, N. G., Zhang, J. H., Liu, D. K., Liu, Q., et al. (2022). Multiobjective optimization algorithm for accurate MADYMO reconstruction of vehicle-pedestrian accidents. *Front. Energy Res.* 10, 1032621. doi:10.3389/fbioe.2022.1032621